Supplementary Information

Supplementary Methods

Supplementary Figures

Supplementary Tables

Supplementary Methods

Materials and Characterization. All chemicals including iron(III) nitrate nonahydrate (catalogue number: 254223), cobalt(II) nitrate hexahydrate (203106) and fumed silica (S5130), iodixanol (D1556), hydrofluoric acid (1.00337) and poly(maleic anhydride-alt-1-octadecene) (419117) were obtained from Sigma-Aldrich unless otherwise stated. TEM images were conducted on a JEM 1230 transmission electron microscope (120 kV). The element mapping was performed by FEI Tecnai F20 TEM (200 kV). UV-vis spectra were carried out on an Agilent spectrophotometer. Dynamic light scattering (DLS) was measured on Malvern ZetaSizer. The iron or cobalt concentrations of samples were measured by an inductively coupled plasma mass spectrometer (ICP-MS, Thermo). Powder X-ray diffraction (XRD) was carried out on a Shimadzu XRD-6000 X-ray diffractometer. Magnetic hysteresis curves were measured via a MicroMag^{TM} (Model 2900, AGM).

In vivo imaging parameters:

CT imaging was performed on a Micro CT (TriFoil Imaging CT120) with fast scan mode. The mice were anesthetized via 2 % isoflurane at 2 L/min of oxygen flow using rodent anesthesia machine (DRE Compact 150) during CT imaging. 3D reconstruction was performed by GE Microview 2.2 and VivoQuant software 2.0.

Thickness: 48 μm;

Voltage: 70kV;

Field of view: 4.0 × 10 cm.

MR imaging was performed on a 3T-MRI scanner (MR solution, MRS 3000) using T_2 sequence. Date analysis was performed using Clear Canvas Worksation software 7.0. For T_2-MRI imaging, mice (n = 4) were place into a mouse body coil and anesthetized with 2% isoflurane at 2 L/min of oxygen flow during MR imaging.

Flip: 90^{o};

Trig: 0 ms;

TR: 5000 ms;

TE: 68 ms;

Slice thickness: 1 mm;

DFOV: 4.0 × 4.0 cm.

Photoacoustic imaging was performed by Vevo LAZR photoacoustic imaging system (Visual Sonics Company, Canada). During the experiments, the mice (n = 4) were anesthetized with 2% isoflurane at 2 L/min of oxygen flow. Three tissue sections were collected for measurement of PA signal intensities. The data was analyzed in Vevo LAB software.

Frequency: 21MHz;

Laser fluence: 25 mJ/cm^2;

2D Power: 100%;

PA Power: 100%;

PA Gain: 42 dB;

2D Gain: 18 dB;

Sensitivity: high;

PA Acquisition: single;

Wavelength: 800 or 1064 nm.

Bioluminescence imaging was performed on an IVIS Spectrum optical imaging system (PerkinElmer, USA). Imaging data were analyzed using IVIS Living Imaging 3.0 software (PerkinElmer). 80 μL of D-Luciferin solution (40 mg/mL) was i.p. injected into mice. 10 min later, the mice (n = 4) were anesthetized with 2% isoflurane at 2 L/min of oxygen flow for bioluminescence imaging.

Binning: 0.5 s;

Exposure time: 3 s;

Excitation filter: block;

Field of view: C.

MPI imaging was performed using a MPI scanner (Magnetic Insight Inc, MOMENTUM™ Imager). The frequency of MPI is 45 kHz. The magnetic gradient strength of MPI is 6T/m. During the experiments, the mice (n = 4) were anesthetized with 2% isoflurane at 2 L/min of oxygen flow. To provide an anatomic reference, CT was taken after the MPI scanning. The analysis of MPI imaging data and coregistration of MPI / CT was processed by VivoQuant software 2.0.

For 2D projection MPI scanning:

The projection quality: Best (slowest);

Z field of view: 4 cm for measuring tube, 10 cm for measuring mouse;

HDR/High sensitivity: Default;

Time Estimate: ～2 min for 4 cm, ～5 min for 10 cm.

For 2D Average MPI scanning:

The projection quality: Best (slowest);

Number of scanning: 25 times;

Z field of view: 4 cm for measuring tube;

HDR/High sensitivity: High Sensitivity;

Time Estimate: ～30 min for 4 cm.

For 3D MPI scanning:

The projection quality: Best (slowest);

Number of projections: 75;

HDR/High sensitivity: High Sensitivity;

Z field of view: 10 cm;

Time Estimate: ～80 min for 10 cm scanning.

***In vivo* biodistribution and toxicity studies.** Healthy Balb/c mice were i.v. injected with FeCo@C-PEG (200 μL, 15 mg/kg) and sacrificed at 1st, 7th, 14th, and 28th day (four mice per group) after injection. Another four healthy Balb/c mice were used as the control. Before the mice were euthanatized, blood samples (~ 1 mL) were collected and sent to Hunan slack laboratory animal Co., Ltd. for blood panel analysis and blood chemistry test. Major organs (including heart, liver, spleen, lung and kidney) of those mice were harvested and divided into two halves for histological examination and biodistribution measurement, respectively. For biodistribution measurement, the major organs were solubilized for inductively coupled plasma mass spectrometer (ICP-MS) measurement to determine Co contents in various organs. For histological examination, the major organs were fixed in 4% of formalin, embedded in paraffin, sectioned into 4 μm slices, stained with hematoxylin and eosin (H&E) and observed by a Leica DM4 B microscope (Leica Microsystems GmbH, Wetzlar, Germany).

Supplementary Figures

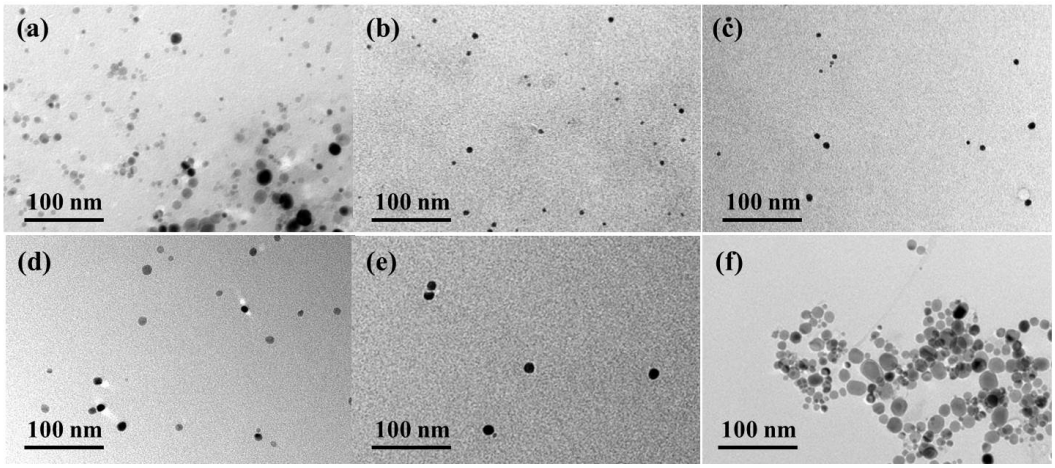

Figure S1. TEM characterization of FeCo nanoparticles. (a) TEM image of FeCo@C-PEG (sample 3) before density gradient separation. (b-f) TEM images of FeCo@C-PEG (sample 3) after density gradient separation: (b) Fraction 1; (c) Fraction 2; (d) Fraction 3; (e) Fraction 4; (f) Fraction 5.

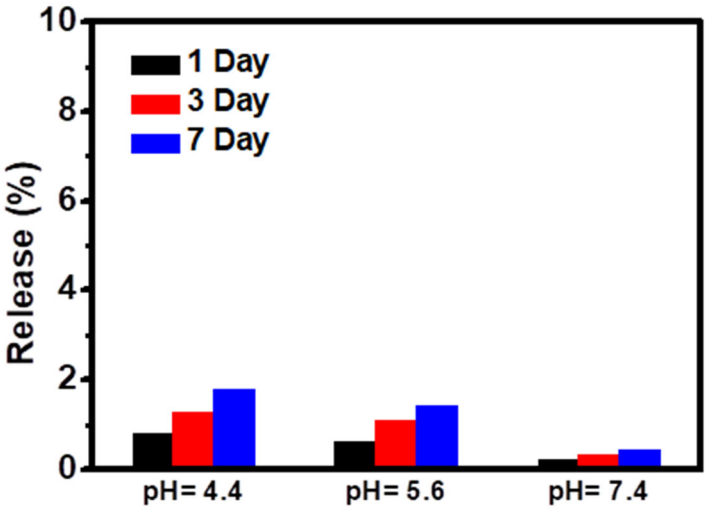

Figure S2. The chemical stability of FeCo@C-PEG. The percentage of Co released from FeCo@C-PEG incubated in 1 x PBS buffers at pH=4.4, pH=5.6 or pH=7.4 for 1, 3 and 7 days, respectively.

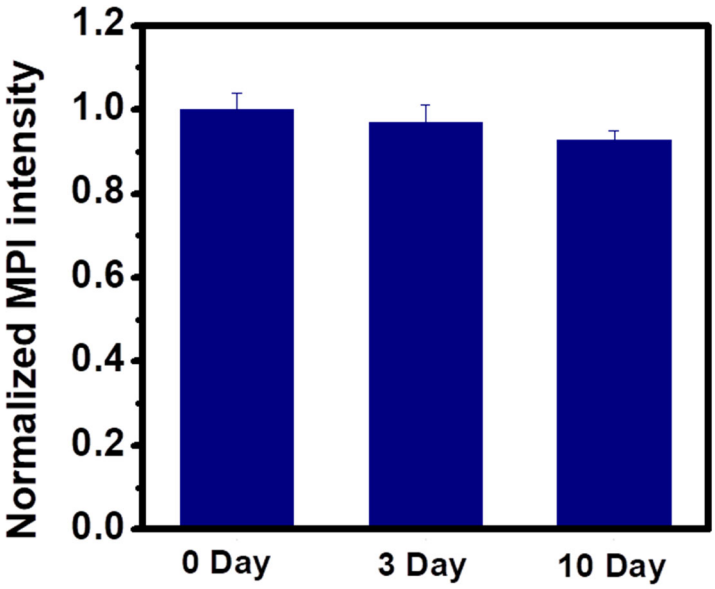

Figure S3. MPI signal stability of FeCo@C-PEG. The normalized MPI signals of FeCo@C-PEG incubated in 1 x PBS buffer (pH = 7.4) for 0, 3, 10 days.

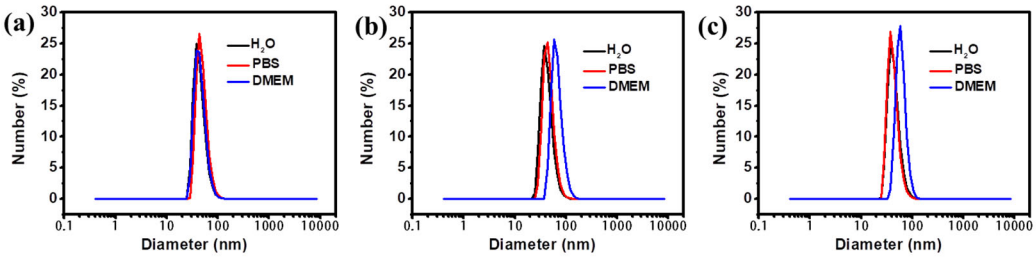

Figure S4. DLS analysis of FeCo@C-PEG incubated in water, 1 x PBS and DMEM for (a) 1 day, (b) 2 days, and (c) 7 days.

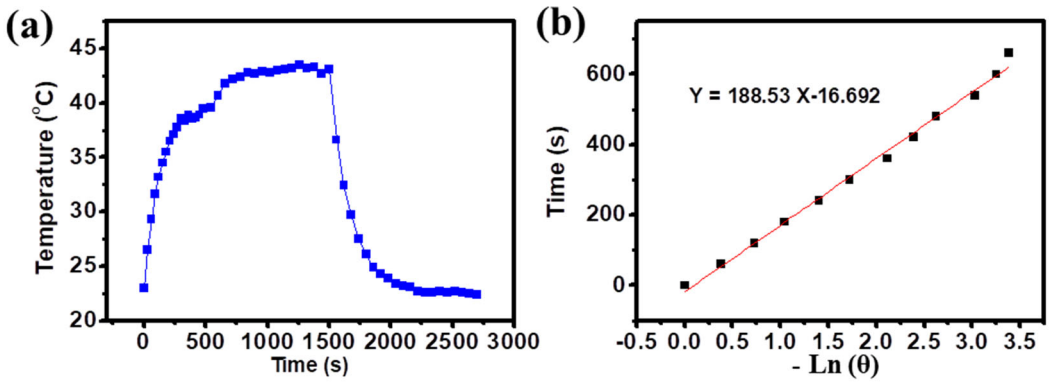

Figure S5 Photothermal conversion efficiency for FeCo@C-PEG. (a) The temperature curve of FeCo@C-PEG aqueous solution, irradiated with 808 nm laser (1 W/cm^2) for 25 min. (b) Plot of cooling time versus negative natural logarithm of the temperature driving force obtained from the cooling stage as shown in (a).

The photothermal conversion efficiency (η) is calculated using **Equation (1)** [1], where h is the heat transfer coefficient; S is the surface area of the container; T_{max} is the equilibrium temperature (T_{max} = 43.1 °C); T_{Surr} is ambient temperature (T_{Surr} = 23.0 °C); Q_{dis} is the heat dissipation from laser absorbed by the sample cell; I is incident laser power; and A_{808} is the absorbance of FeCo@C-PEG at 808 nm (A_{808} = 0.18).

$$\eta = \frac{hS(Tmax-Tsurr)-Qdis}{I\ (1-10^{-A808})} \qquad (1)\ [1]$$

To obtain the value of hS, a dimensionless driving force temperature (θ) and a sample system time constant (τs) is introduced using **Equation (2)** and **(3)**. τs for heat transfer from the system is determined to be 188.53 by applying the linear time data from the cooling period (after 1500 s) vs negative natural logarithm of driving force temperature (**Figure S5b**).

$$\theta = \frac{T-Tsurr}{Tmax-Tsurr} \qquad (2)\ [1]$$

$$t = -\tau s \cdot \ln\theta \qquad (3)\ [1]$$

The value of hS is derived from **Equation (4)**, where Mw is the mass of solvent (M_w = 0.2 g), C_w is the heat capacity of solvent (C_w = 4.2 J g^{-1} K^{-1}), to be 0.00446.

$$\tau s = \frac{Mw \cdot Cw}{hS} \qquad (4)\ [1]$$

The Q_{Dis} was measured independently using a sample cell containing water (Q_{Dis} = 0.00137 W). Therefore, the photothermal conversion efficiency (η) was calculated to be 26.7 % by **Equation (1)**.

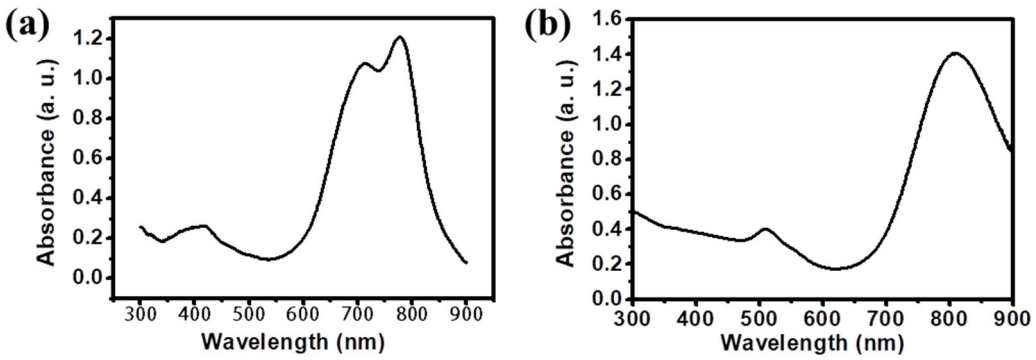

Figure S6. The absorption spectra of (a) indocyanine green (ICG) and (b) Au nanorods. Au nanorods were prepared according to the seed growth method.[2]

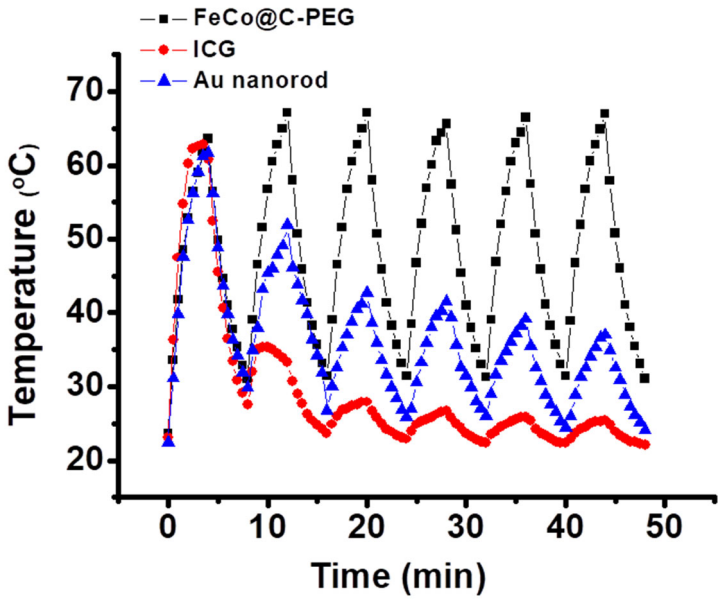

Figure S7. Photothermal stability of FeCo@C-PEG. Reversible heating-cooling of FeCo@C-PEG, Au nanorods and indocyanine green (ICG). In each heating-cooling circle, the solution was irradiated by 808 nm laser for 4 min and then cooled down for another 4 min.

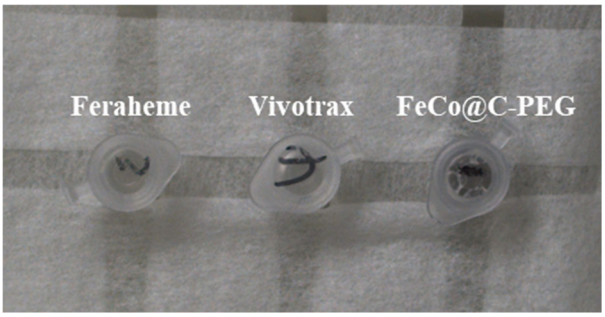

Figure S8. Photograph of FeCo@C-PEG, Vivotrax and Feraheme (800 ng of core) in PCR tubes for MPI scanning.

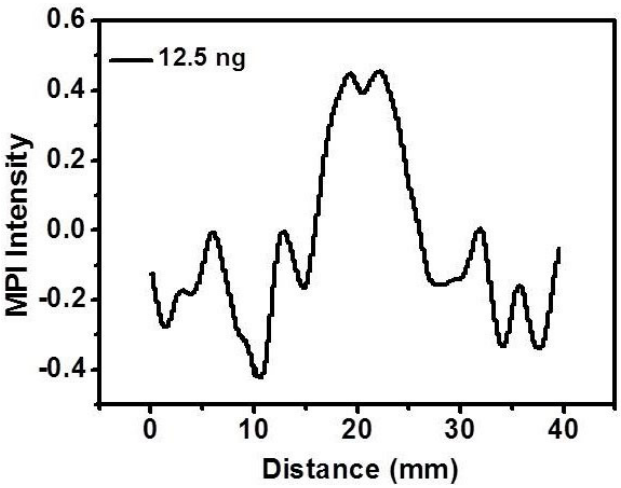

Figure S9. MPI spectrum (single scan) of a PCR tube containing FeCo@C-PEG (12.5 ng of core).

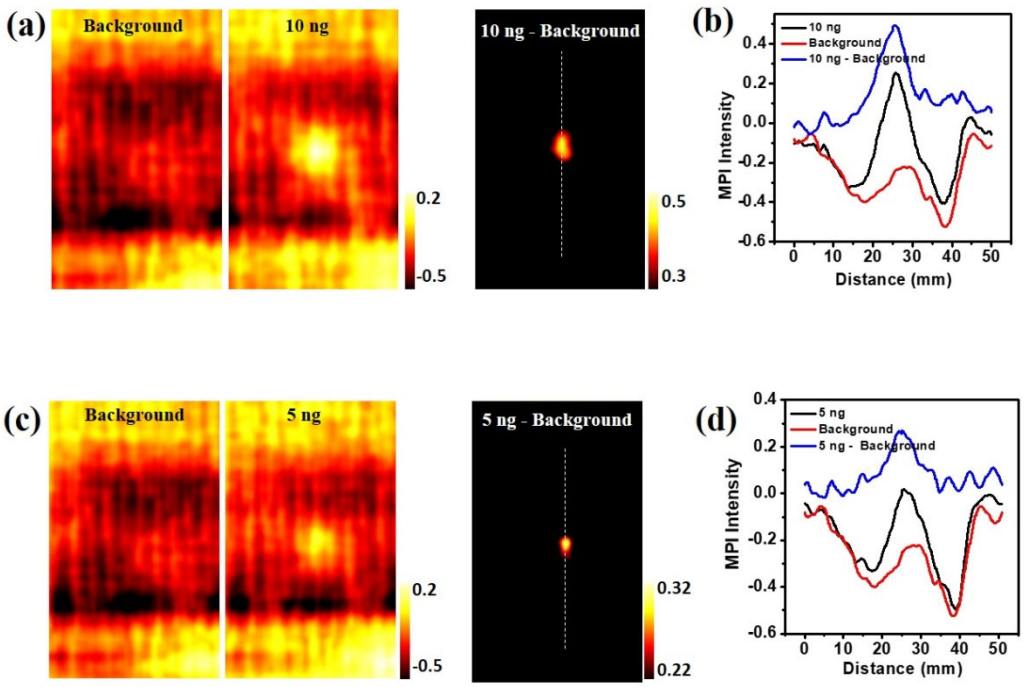

Figure S10. High sensitivity MPI imaging of FeCo@C-PEG. (a) 2D Average MPI images (25 times scanning) of PCR tube containing 0 ng and 10 ng of FeCo@C-PEG as “background” and “10 ng”, respectively; Subtraction of the image of “background” from the image of “10 ng” afforded the corrected MPI images of “10 ng – background”. (b) Corresponding MPI spectra of “background”, “10 ng” and “10 ng – background”. (c) 2D Average MPI images (25 times scanning) of PCR tube containing 0 ng and 5 ng of FeCo@C-PEG as “background” and “5 ng”, respectively; Subtraction of the image of “background” from the image of “5 ng” afforded the corrected MPI images of “5 ng – background”. (d) Corresponding MPI spectra of “background”, “5 ng” and “5 ng – background”.

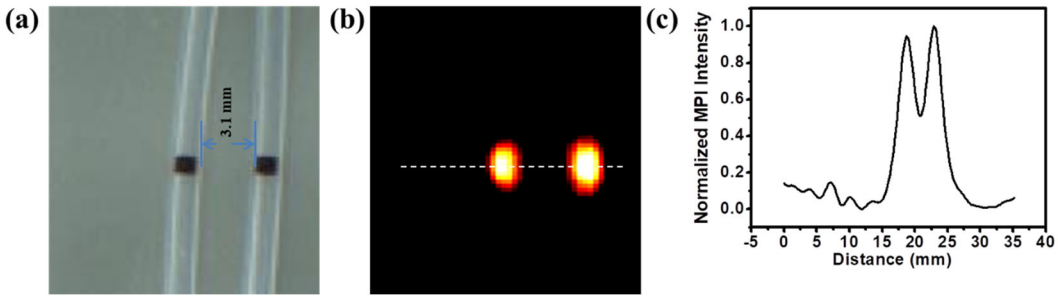

Figure S11. The resolution of MPI images of FeCo@C-PEG nanoparticles, according to the literature report method.[3] Two microbore tubes were filled with 0.5 μL of FeCo@C-PEG and were parallelly arranged in a linear array with an edge-to-edge distance of 3.1 mm between these two tubes. (a) Photograph. (b) Two-dimensional MPI image. (c) Linear scanning MPI spectrum.

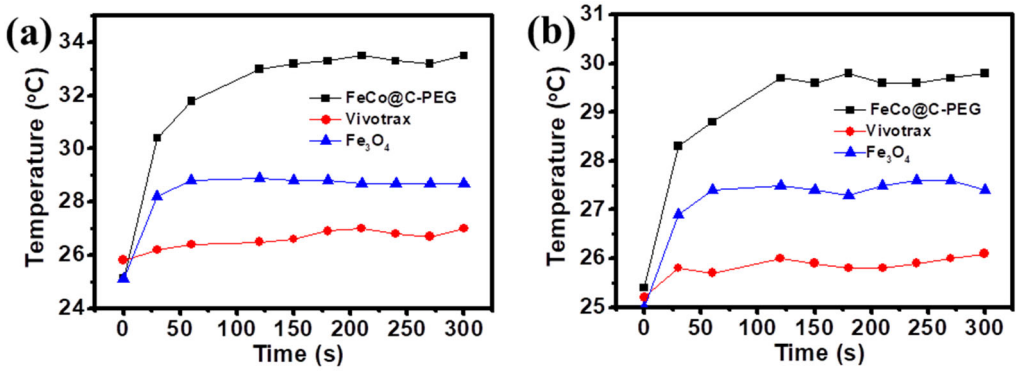

Figure S12. Magnetic hyperthermia heating curves of FeCo@C-PEG (Fraction #3), Vivotrax and Fe_3O_4 nanoparticles, measured inside the magnetic hyperthermia coil setup (100 kHz, 15 KVA): (a) 2 mg/mL core concentration; (b) 1 mg/mL core concentration. Fe_3O_4 nanoparticles was prepared by the co-precipitation method according to the literature report. [4]

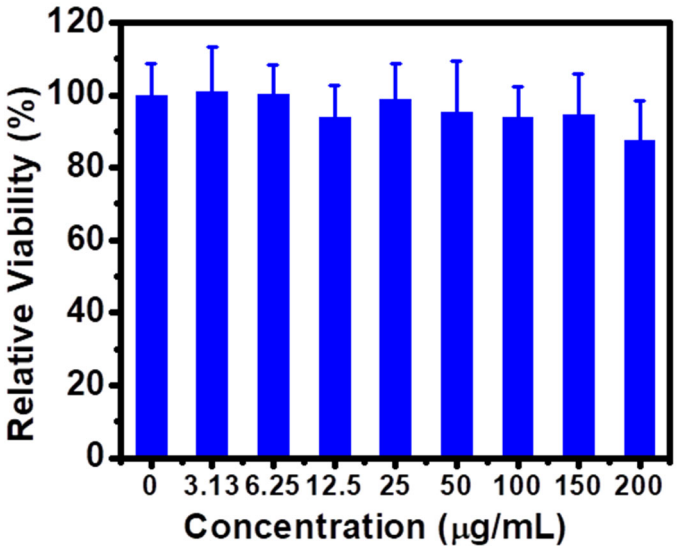

Figure S13. Relative viabilities of 4T1 cancer cells incubated with FeCo@C-PEG with different concentrations for 24 h, measured by the MTT assay.

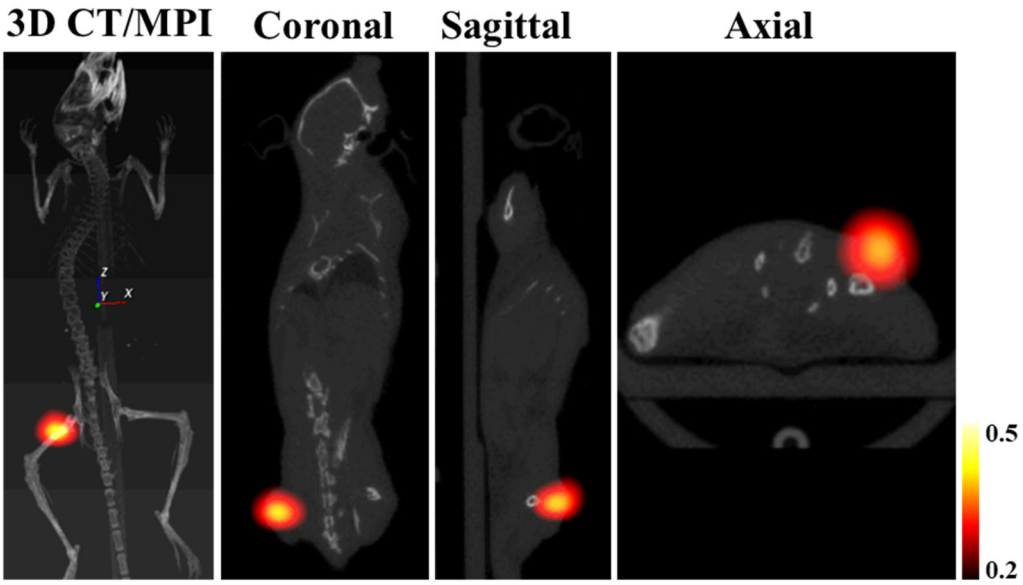

Figure S14. 3-D projection MPI/CT images, coronal, sagittal, and axial images of a mouse bearing a 4T1 xenograft breast tumor and receiving an intratumoral injection of FeCo@C-PEG.

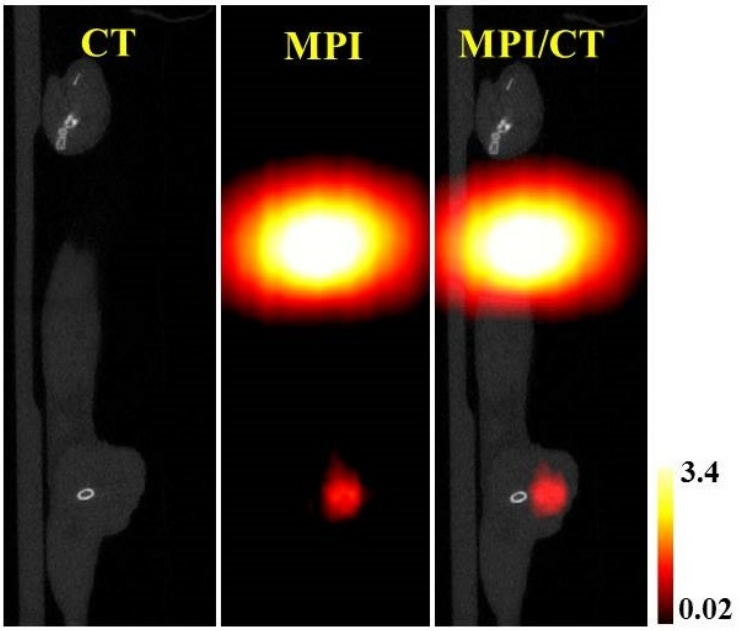

Figure S15. The mice bearing 4T1 xenograft breast tumors were i. v. injected with 0.2 mL of FeCo@C-PEG (0.3 mg/mL): Sagittal CT, MPI, and CT/MPI images of mice 24 hours after injection.

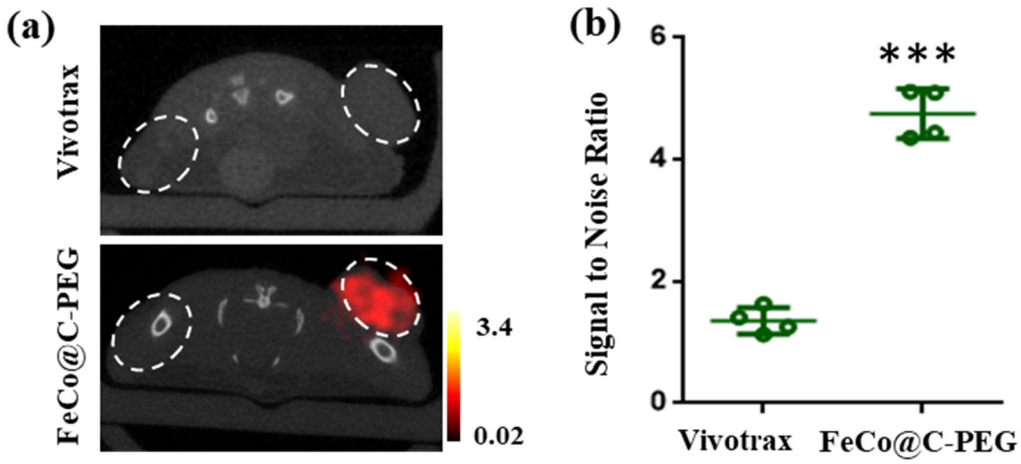

Figure S16. Signal-to-background ratio of MPI imaging of tumor. (a) Axial MPI/CT images of mice at 24 h post i.v. injection of Vivotrax (3 mg/kg) or FeCo@C-PEG (3 mg/kg). Left marked area indicated normal tissue; the right marked area indicated tumor. (b) Signal-to-background ratio calculated from the MPI signals of marked tumor areas and marked normal tissues in (a) (Two-tailed Student's t-test, ***P = 0.0003, error bars represent mean ± s. d., n = 4).

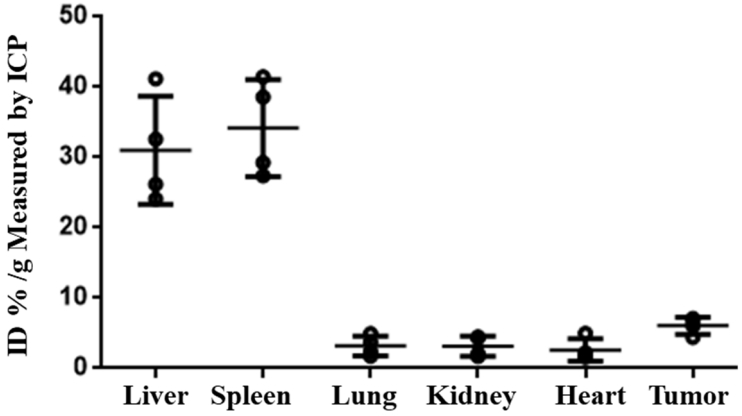

Figure S17. The biodistribution of FeCo@C-PEG measured by ICP-MS in Balb/c mice bearing 4T1 tumor i.v. injected with FeCo@C-PEG (3 mg/kg) and sacrificed at 24 h after injection. Major organs of those mice were harvested and solubilized for ICP-MS measurement to determine Co contents.

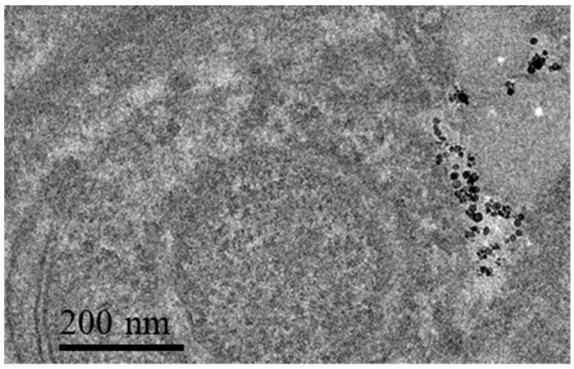

Figure S18. Bio-TEM image of 4T1 tumor slice showed the nanoparticles within the tumor. Balb/c mice bearing 4T1 tumors were i.v. injected with FeCo@C-PEG (3 mg/kg). 24 h later, the tumor was removed, fixed, sliced, and stained for Bio-TEM characterization.

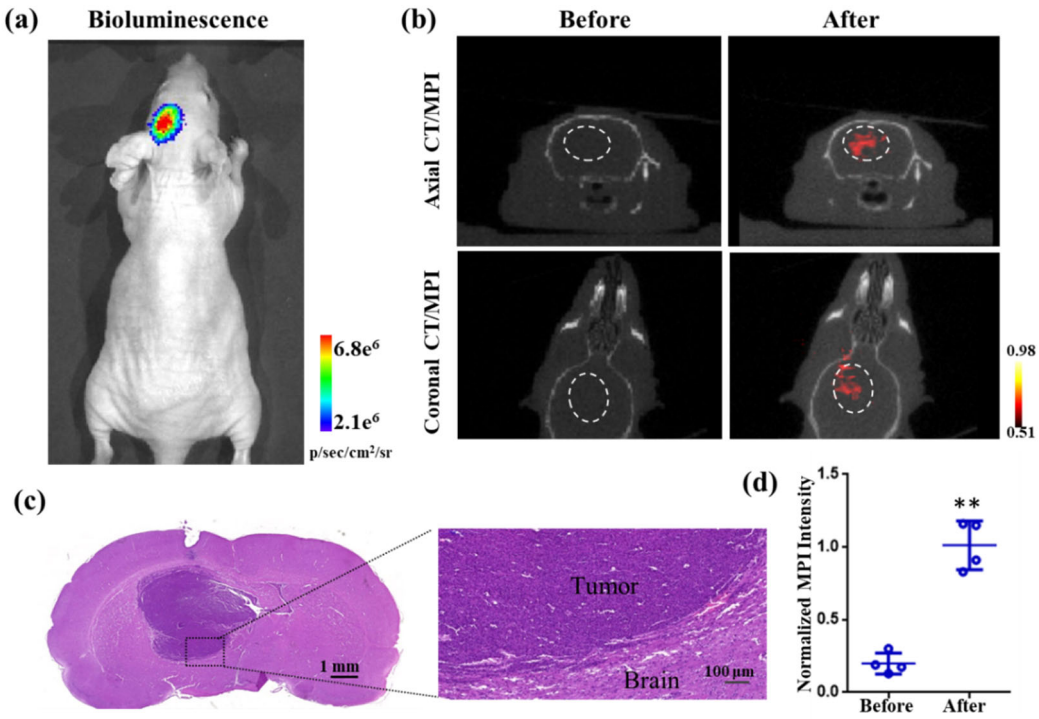

Figure S19. Imaging of orthotopic brain tumor xenografts in mice. (a) Representative bioluminescence image of a mouse with an orthotopic brain tumor (U87-luciferase cell line). (b) Axial and coronal MPI/CT images of mice before and after injection of FeCo@C-PEG (9 mg/kg). (c) Haematoxylin and Eosin (H&E) staining of brain slice. (d) Corresponding quantification of MPI signals from marked tumor areas (b) (Two-tailed Student's t-test, **P = 0.0011, error bars represent mean ± s. d., n = 4).

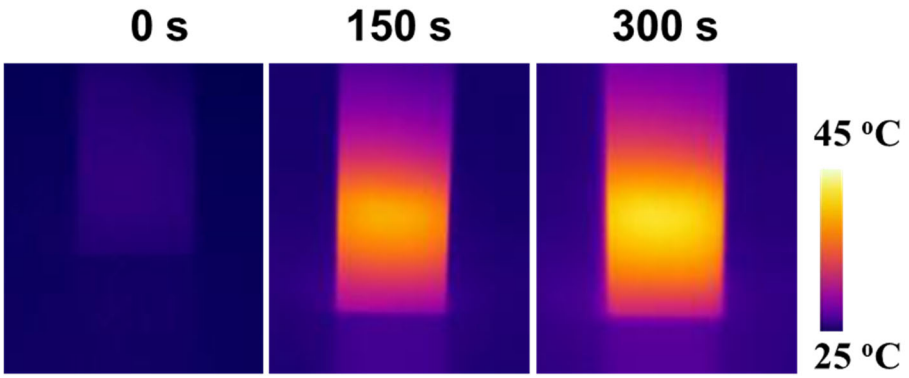

Figure S20. Thermal images of FeCo@C-PEG (220 μg/mL) under 1064 nm laser irradiation (1.0 W/cm^2) for indicated periods of time.

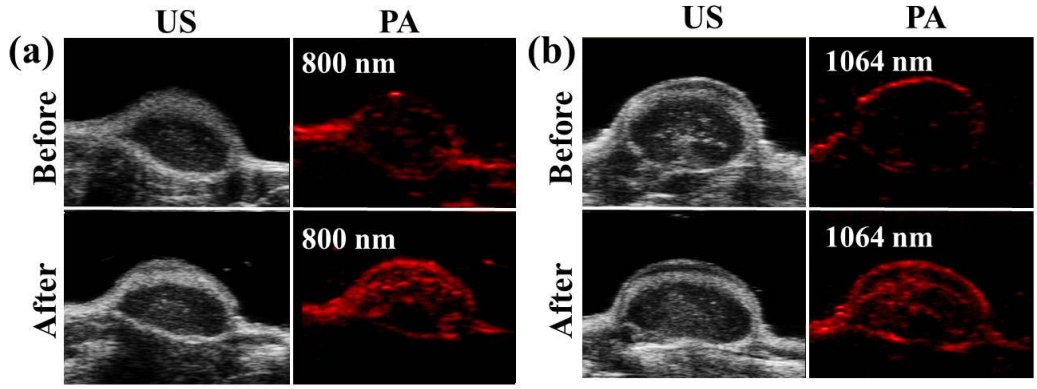

Figure S21. The mice bearing 4T1 tumors were scanned by a PA imager before and after i. v. injection of FeCo@C-PEG. (a) US and PA images scanned at 800 nm laser excitation; (b) US and PA images scanned at 1064 nm laser excitation.

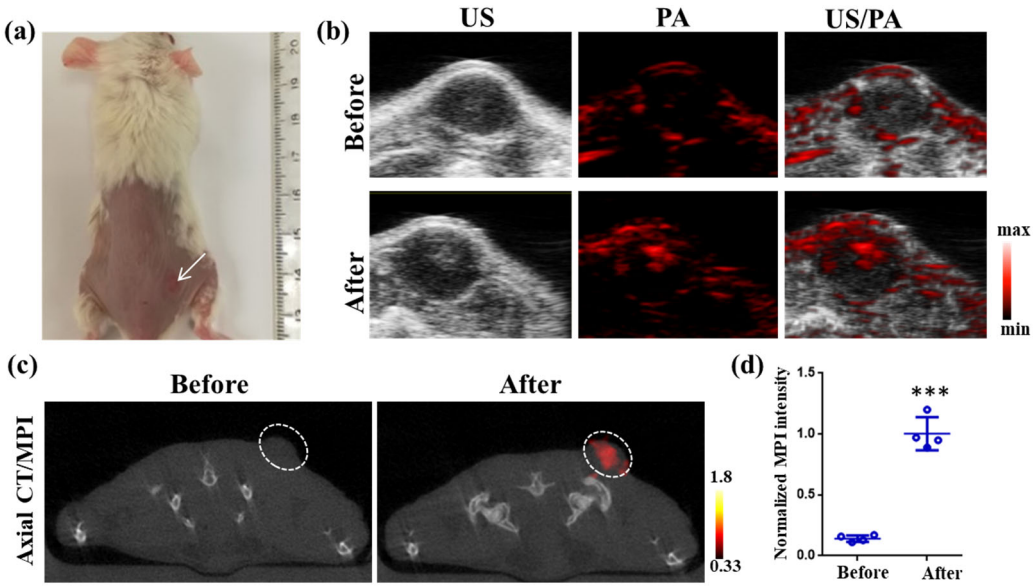

Figure S22. MPI and PA imaging of mice bearing small tumor. (a) Photograph of representative Balb/c mouse bearing a 4T1 xenograft breast small tumor (diameter: about 4 mm). Those mice were i.v. injected with FeCo@C-PEG (3 mg/kg) (n = 4). (b) US/PA images of mice before and 24 h post injection at 800 nm of laser excitation. (c) Axial CT/MPI images before and 24 h after injection. (d) Normalized MPI signals of marked tumor areas before and after injection. (Two-tailed Student's t-test, ***P = 0.00064, error bars represent mean ± s. d., n = 4).

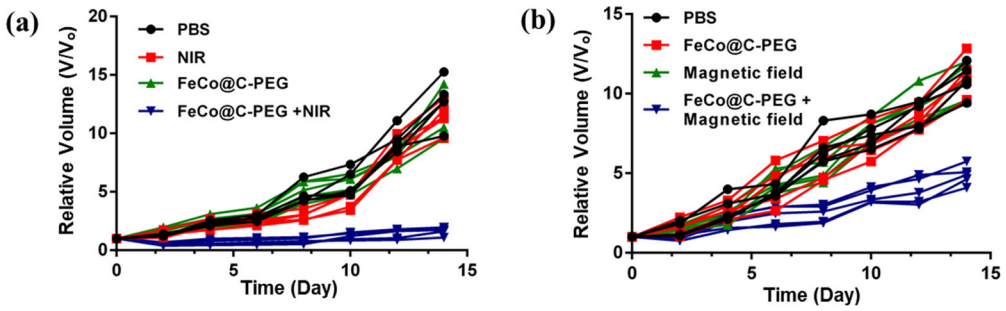

Figure S23. The growth curves of tumor xenografts in mice receiving (a) photothermal therapy and (b) magnetic hyperthermia therapy.

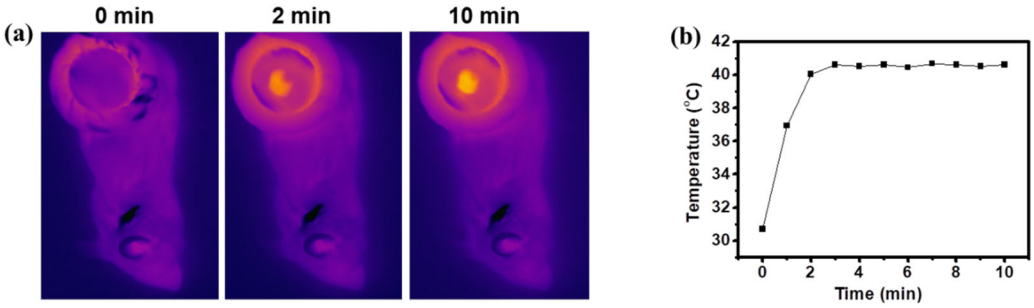

Figure S24. (a) Infrared thermal images of tumor-bearing mice i. t. injected with FeCo@C-PEG (50 μL, 2 mg/mL, 100 μg), and then heated in a magnetic coil setup (100 kHz, 15 KVA). (b) Corresponding magnetic hyperthermia heating curve of tumor monitored by the infrared thermal camera.

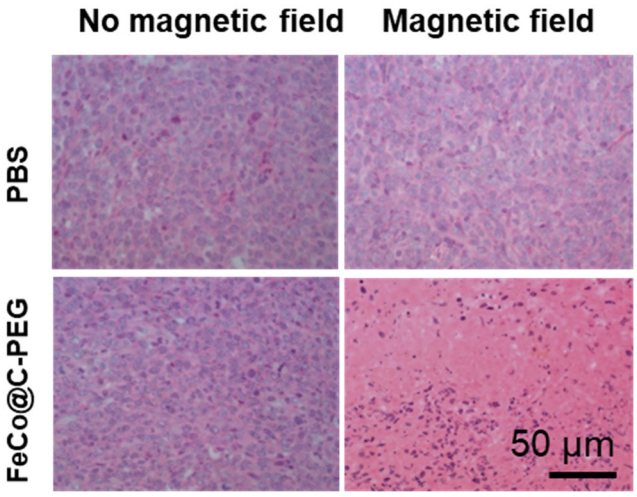

Figure S25. Micrographs of H&E staining of tumor slices collected from mice treated with 1 x PBS, Magnetic field (100 kHz, 15 KVA) only, FeCo@C-PEG only (i. t. injection, 50 μL, 5 mg/mL), and FeCo@C-PEG (i. t. injection, 50 μL, 5 mg/mL) + Magnetic field (100 kHz, 15 KVA).

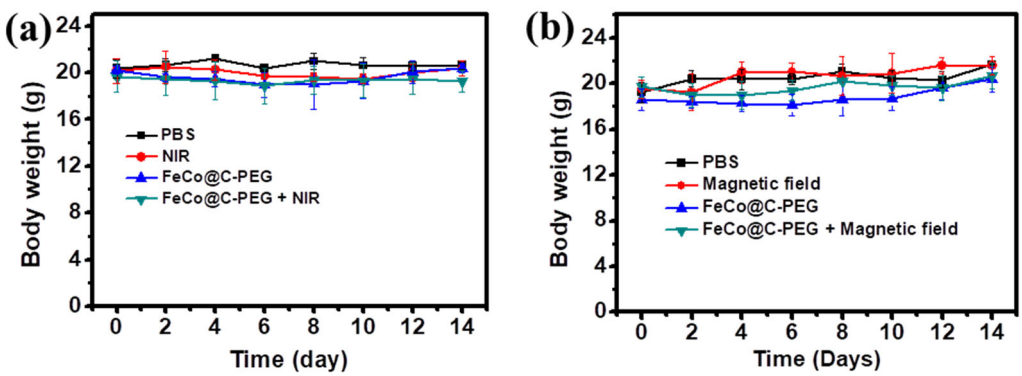

Figure S26. Body weights of mice from different groups as indicated after (a) photothermal therapy and (b) magnetic hyperthermia therapy.

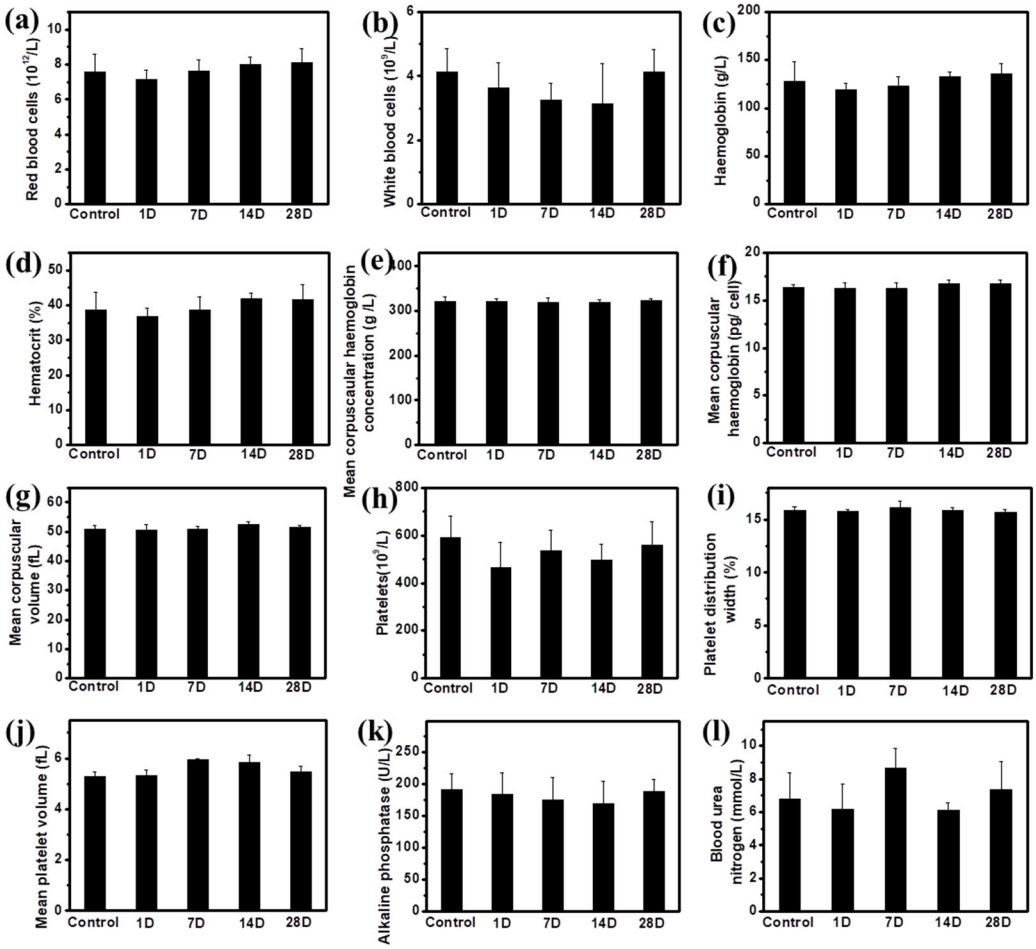

Figure S27. Complete blood panel and blood biochemistry analysis of mice i. v. injected with FeCo@C-PEG (15 mg/kg) at various time points (1st, 7th, 14th, and 28th day). The examined parameters included (a) Red blood cell (RBC) counts; (b) White blood cell (WBC) counts; (c) Hemoglobin (HGB); (d) Hematocrit (HCT); (e) Mean corpuscaular haemoglobin concentration (MCHC); (f) Mean corpuscular hemoglobin (MCH); (g) Mean corpuscular volume (MCV); (h) Platelets (PLT); (i) Platelet distribution width (PDW); (j) Mean platelet volume (MPV); (k) Alkaline phosphatase (ALP); (l) Blood urea nitrogen (BUN).

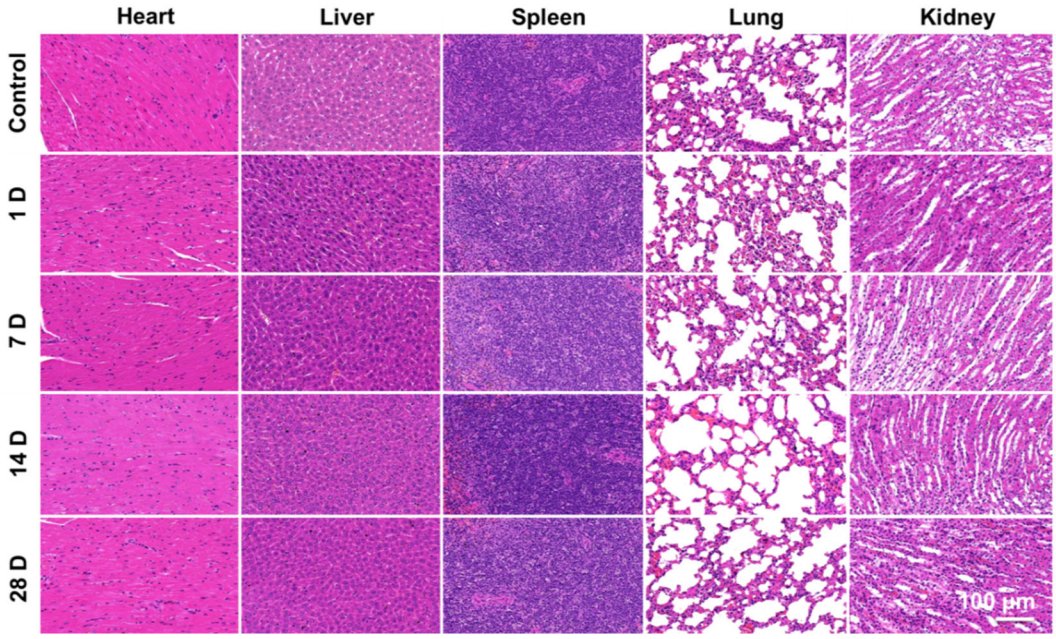

Figure S28. H&E-stained tissue sections of major organs including heart, liver, spleen, lung and kidney of mice receiving intravenous injection of FeCo@C-PEG (15 mg/kg). Those mice were examined on the 1st, 7th, 14th, and 28th day post injection. Untreated healthy mice were used as the control.

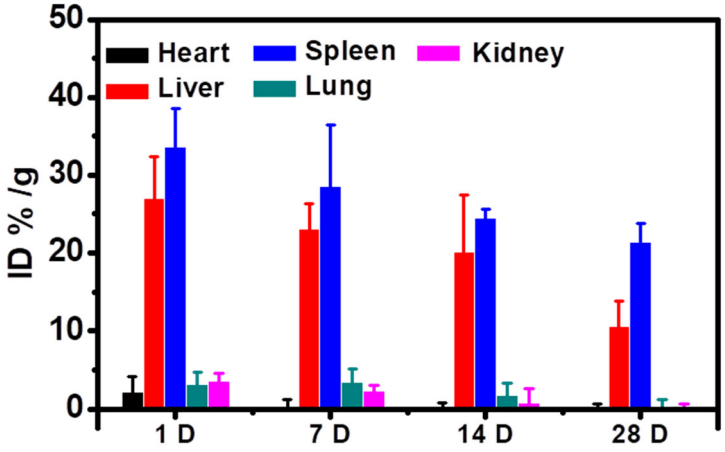

Figure S29. The time-dependent biodistribution of FeCo@C-PEG. After i. v. injection of FeCo@C-PEG (15 mg/kg), the major organs of mice (including heart, liver, spleen, lung and kidney) were collected at the 1st, 7th, 14th, and 28th day for ICP-MS measurement of Co levels to determine the biodistribution of nanoparticles.

Supplementary Tables

	FeCo@C-PEG	Vivotrax	Fe_3O_4
SAR (w/g)	406	84	266

Table S1. The specific absorption rate (SAR) of magnetic hyperthermia for FeCo@C-PEG, Vivotrax and Fe_3O_4 (100 KHz). SAR is defined as the absorbed energy per material mass, expressed as watt per gram (W/g).[5] SAR was calculated by the **Equation 5**, where $M_{(FeCo)}$ is the total mass of FeCo in the sample, Cw is water heat capacity (*C*w = 4.18 J g^{-1} K^{-1}), Mw is the mass of solvent. From the magnetic hyperthermia curves (Supplementary Fig. S12b), the temperature elevation was measured as a function of time (dT/dt) at the initial linear slope (t = 30 s).

$$\mathrm{SAR} = \frac{\mathrm{Mw \cdot Cw}}{\mathrm{M(FeCo)}} \cdot \frac{\mathrm{dT}}{\mathrm{dt}} \qquad (5)$$ [5]

Concentration (μg/mL)	20	60	100	220
SAR (w/g)	14700	3150	3990	3150

Table S2. The SAR of photothermal hyperthermia for FeCo@C-PEG at different concentrations under irradiation of 1064 nm laser (1.0 W/cm^2). From the temperature curves (**Fig. 4d** in main text), SAR for FeCo@C-PEG was calculated using the Equation (5)[5], where $M_{(FeCo)}$ is the total mass of FeCo in the sample, Cw is water heat capacity (*C*w = 4.18 J g^{-1} K^{-1}), Mw is the mass of solvent, the temperature elevation is measured as a function of time (dT/dt) at the initial linear slope (t = 20 s).

References

1. Roper, D.K., Ahn, W. & Hoepfner, M. Microscale heat transfer transduced by surface plasmon resonant gold nanoparticles. *J. Phys. Chem. C* **111**, 3636-3641 (2007).
2. Qiwei, T.*, et al.* Hydrophilic Cu_9S_5 nanocrystals: a photothermal agent with a 25.7% heat conversion efficiency for photothermal ablation of cancer cells in vivo. *ACS Nano* **5**, 9761-9771 (2011).
3. Ferguson, R.M.*, et al.* Magnetic particle imaging with tailored iron oxide nanoparticle tracers. *IEEE T. Med. Imaging* **34**, 1077-1084 (2015).
4. Tay, Z.W.*, et al.* Magnetic particle imaging-guided heating in vivo using gradient fields for arbitrary localization of magnetic hyperthermia therapy. *ACS Nano* **12**, 3699-3713 (2018).
5. Espinosa, A.*, et al.* Magnetic (hyper)thermia or photothermia? Progressive comparison of iron oxide and gold nanoparticles heating in water, in cells, and in vivo. *Adv. Funct. Mater.* **28**, 1803660 (2018).